Clays and Clay Minerals (2024), **72**, e17, 1–12
doi:10.1017/cmn.2024.28

Original Paper

Smectite–brine–CO_2 interactions: effects of interlayer chemistry, brine concentration, CO_2 pressure, and temperature

Paolo Andre Benavides and Stephen Guggenheim

Department of Earth and Environmental Sciences, University of Illinois at Chicago, Chicago, IL 60607, USA

Abstract

Smectite may impact the ability of saline aquifer–caprock systems to store CO_2 effectively, because of changes in pressure, temperature, and brine concentration induced by the injection of CO_2. These changes influence the molar volume of smectite, affecting the short-term structural and stratigraphic trapping, or the dissolution of smectite via the long-term geochemical trapping. This study investigated the d_{001} value of an interlayer-cation-exchanged smectite, Na-rich SWy-2 (Na-SWy-2), with Ca or Mg (hereafter CaSWy-2 and MgSWy-2). Molar volume experiments used X-ray diffraction and a high-pressure environmental chamber. The extent of smectite dissolution was simulated at experimental conditions by geochemical modeling using a rate equation derived from the transition state theory. CaSWy-2-$CaCl_2$ and MgSWy-2-$MgCl_2$ brine systems showed that increasing the brine concentration from 0.17 M to saturation results in a ≤18% decrease in d_{001} values, and increasing the temperature from approximately 33 to 150°C results in ≤11% decrease. The effect of the interlayer cation shows the d_{001} values of MgSWy-2 are ≤0.4 Å higher compared with CaSWy-2. Geochemical modeling shows the extent of dissolution of Na-SWy-2, CaSWy-2, or MgSWy-2 is only ≤1.1% in acidic conditions. Furthermore, the calculated swelling pressure needed to decrease the H_2O sheets in the interlayer, from 3W to 2W, of MgSWy-2 and CaSWy-2 are higher compared with Na-SWy-2. The swelling pressure was approximated from the sum of the osmotic repulsive pressure, the van der Waals attractive pressure, and the hydration pressure. The data suggest that Na-SWy-2, CaSWy-2, and MgSWy-2 may affect saline aquifer–caprock systems to store CO_2. The molar volume is affected by changes in pressure, temperature and brine concentration, or swelling pressure from the injection of CO_2. An increase in the d_{001} value of SWy-2 can enhance the sealing capabilities of a caprock by making saline aquifers less porous and less permeable and thus increasing the capability for CO_2 storage. In contrast, a decrease in the d_{001} value can create cracks in a caprock and thus provide conduits for the CO_2 to escape. Furthermore, the CO_2 injection will cause a decrease in pH, causing smectite to dissolve until it reaches a steady state. However, despite acidic aquifer conditions, SWy-2 has low solubility.

Keywords: activity of water; caprock; CO_2 storage; interlayer cation; saline aquifer; smectite; solubility; swelling pressure

(Received: 09 April 2024; revised: 03 June 2024; accepted: 14 June 2024)

Introduction

Since the 1700s, atmospheric carbon dioxide (CO_2) concentration has increased by 49% because of land-use change, and use of coal and fossil fuels as a form of energy (Friedlingstein et al., 2019). To mitigate the anthropogenic increase of CO_2, one proposed strategy is to capture and store CO_2 in deep saline aquifers (IPCC, 2007). Deep saline aquifers are excellent candidates to contain CO_2 because of their high storage capacity (to 10,000 Gt of CO_2), easy access near CO_2 capture sites, and high porosity and permeability (Davidson et al., 2001). When supercritical CO_2 ($scCO_2$) is injected, the $scCO_2$ migrates upwards, displacing the brine. The saline aquifer requires an impermeable caprock, which may be composed of evaporites (anhydrites or halites), carbonates (limestones or dolostones), or argillaceous rocks (clay-rich shales and mudstones) to effectively store the injected $scCO_2$ (Song and Zhang, 2013).

Most current and future CO_2 storage sites are sandstone aquifers sealed by clay-rich shale caprocks (Michael et al., 2010). Both sandstone and shale may contain smectite, a swelling clay mineral. Smectite often occurs in sandstones as a detrital sand-grain coating (Baker et al., 1993), whereas in shales, smectite is a main component. The interlayer distance (d_{001}) of the smectite changes as the activity of H_2O ($a(H_2O)$) varies, which is affected by the brine chemistry, pressure, and temperature. Because smectite is often found in pore spaces of sandstones, changes in d_{001} of smectite may affect the porosity and permeability in the sandstone reservoir, impacting its CO_2 storage capacity, and causing shrinkage and microfracturing in shales.

Laboratory experiments were performed previously to investigate the effect of changes in brine concentration, pressure, and/or temperature on the d_{001} of smectite. Norrish (1954) first showed that increasing NaCl brine concentration decreases the d_{001} of smectite, and this result was further supported by Slade et al.

Corresponding author: Paolo Andre Benavides; Email: pbenav2@uic.edu

Cite this article: Benavides P.A., & Guggenheim S. (2024). Smectite–brine–CO_2 interactions: effects of interlayer chemistry, brine concentration, CO_2 pressure, and temperature. *Clays and Clay Minerals* **72**, e17, 1–12. https://doi.org/10.1017/cmn.2024.28

(1991) using varied brine compositions and smectite samples. The effect of CO_2 pressure and temperature on Na-rich smectite (SWy-2) was studied by Giesting et al. (2012a), and on K- and Ca-exchanged smectite by Giesting et al. (2012b). They found that smectite with 0 to 1 plane of H_2O in the interlayer (0W to 1W) allowed CO_2 to migrate in the smectite interlayer to cause swelling. By investigating smectite with a different interlayer H_2O content, Loring et al. (2013) found that CO_2 adsorption is at a maximum with 1W, and decreases with increasing interlayer H_2O content. However, these previous studies were performed under dry to limited H_2O conditions, i.e. relative humidity <100%.

In situ X-ray measurements of smectite under water-saturated conditions present several experimental difficulties. These difficulties include smectite flocculation when in contact with brine and a low signal-to-noise ratio from the effect of the liquid dispersing X-rays. In addition, reactions between smectite and its environment are rapid and non-quenchable. Using a high-pressure environmental chamber (HPEC) developed by Guggenheim and Koster van Groos (2014), Benavides et al. (2020) were able to resolve these problems. They investigated the molar volume, i.e., of Na-rich smectite by simulating environmental conditions relevant to CO_2 storage: CO_2 pressure ($P(CO_2)$ = ambient to 500 bars), temperature (T = ~33 to 150°C), and NaCl brine concentration (0.17 M to saturation). They found that the d_{001} of Na-rich smectite is significantly affected by brine concentration and T compared with $P(CO_2)$. Benavides et al. (2020) also found that Na-rich smectite has hydration levels of more than two interlayer H_2O planes (>2W), and CO_2 does not migrate into the interlayer, which supports the study by Loring et al. (2013).

Studies with smectite–scCO_2/CO_2–brine systems under water-saturated conditions were carried out using NaCl and KCl brines (e.g. Benavides et al., 2020), but CO_2 storage-site brines may also contain other cations and anions. Smectite in such storage sites may undergo cation exchange, thereby changing the interlayer cation composition, e.g. Na in the smectite may be partially replaced by Ca. The interlayer cation composition affects the interlayer distance of smectite because cations have different hydration energies. The hydration energy of a cation is a function of its charge and size, where a smaller cation with a higher charge (e.g. Mg) attracts H_2O more strongly compared with a larger cation with a lower charge (e.g. Na). Ferrage et al. (2005) examined the hydration of smectites with different interlayer cation compositions. They found that hydration of smectites may be affected by the ionic potential (charge to size ratio) of the cation, which is consistent with similar studies (e.g. Sato et al., 1992). Furthermore, Ferrage et al. (2005) observed that there is heterogeneity in the hydration levels of smectite. With increasing relative humidity, smectites with greater interlayer cation ionic potential (i.e. more cations with small size and greater charge) have greater proportions of 2W hydration than 1W and 0W compared with smectite with smaller interlayer cation ionic potential. Slade et al. (1991) investigated smectites with different interlayer cation compositions in brines, e.g. Ca-exchanged smectite with $CaCl_2$ brine. They found that osmotic pressure, directly related to $a(H_2O)$, required to decrease the hydration level from 3W to 2W of smectite is related to the size and charge of the cation in both the brine and the interlayer. Hence, including the effect of the interlayer cation composition would add a better understanding of smectite–scCO_2/CO_2–brine systems.

When CO_2 is injected in saline aquifers, environmental conditions change which affects the interlayer (i.e. layer-to-layer) distance of smectite and the stratigraphic- and structural-trapping CO_2 storage mechanism. These changes in smectite can affect the porosity and permeability of the aquifer and caprock. Stratigraphic and structural trapping are the main CO_2 storage mechanism for the first 10 years after CO_2 injection stops. Over time, the trapping mechanism becomes dominated by geochemical trapping by which the injected CO_2 dissolves in the brines in the formation (solubility trapping) or reacts with other dissolved ions and mineral phases to form carbonate minerals (mineral trapping) (IPCC, 2007). Based on a solubility model by Duan and Sun (2003), the CO_2 solubility in brine decreases with temperature and brine concentration, and increases with pressure. This model is supported by Shao et al. (2013), whose *in situ* pH measurements are comparable to the pH values they calculated with modeling programs (e.g. PHREEQC) using the CO_2 solubility model by Duan and Sun (2003).

Dissolution of CO_2 in the brines in the formation forms carbonate (CO_3^{2-}) and hydrogen ions (H^+), and results in an increase in the activity of H^+ ($a(H^+)$), causing a decrease in pH. The measured and calculated pH values in CO_2 storage site conditions range from 2.9 to 3.7 (Shao et al., 2013). Zysset and Schindler (1996) performed dissolution experiments with K-exchanged smectite in varying KCl solutions within a pH range of 1.0–6.0, and found that the edge sites of the smectite become protonated, i.e. H^+ ion adsorption, which promotes the dissolution of K-rich smectite. Stadler and Schindler (1993) showed that the density of protonated edges increases with $a(H^+)$, i.e. decrease in pH. In studies with CO_2 storage sites, the decrease in pH associated with the CO_2 injection promotes the dissolution of K-rich feldspars and plagioclase feldspars, which contributes to the precipitation of carbonates and clay minerals, such as smectite. This was observed using *in situ* laboratory (e.g. Wigand et al., 2008) and geochemical modeling data (e.g. Ilgen and Cygan, 2016).

The purpose of the present study expands the work of Benavides et al. (2020) on the effects of changes in pressure, temperature, and brine concentration on the d_{001} of smectite using the HPEC by including the effect of divalent cations, Ca and Mg, in the interlayer. These cations are in saline aquifer brines, e.g. in the Utsira Formation at the Sleipner CO_2 storage site in the North Sea (Gregersen et al., 1998). Furthermore, the long-term stability of smectite in deep saline aquifers under a wide range of environmental conditions is investigated using geochemical modeling. Although K is also a common cation in saline aquifer brines, K-exchanged smectite in KCl brines is not studied further because K-exchanged smectite lacks periodicity owing to random interstratification of layers with varying hydration levels and no diagnostic d_{001} X-ray peak (Benavides et al., 2020).

Materials and methods

Starting material

The starting material was a natural, Na-rich smectite (montmorillonite), SWy-2, obtained from the Source Clays Repository of The Clay Minerals Society. Because SWy-2 contains soluble salts and larger-grain minerals, 50 mg of SWy-2 was purified by sonification in 50 mL of distilled water followed by centrifugation. The process was repeated five times until the supernatant no longer reacted with $AgNO_3$ with visible AgCl precipitates. The <2 μm size fraction of the purified SWy-2 was obtained by following the procedure of Moore and Reynolds (1997; pp. 211–213). The Ca- and Mg-exchanged SWy-2 (hereafter CaSWy-2 and MgSWy-2, respectively) were obtained by saturating and agitating via sonification of the <2 μm SWy-2 with 0.10 M $CaCl_2$ or 0.10 M $MgCl_2$ made using high-purity (99.99%)

salts, respectively, and letting the mixture sit at room temperature for 24 h. This process was repeated two more times to ensure complete cation exchange. To remove excess salt, the cation-exchanged smectite was purified using the same procedure as with the starting material, and then dried under ambient conditions and stored in a glass vial.

Equipment

In situ X-ray diffraction (XRD) experiments of a smectite–brine–CO_2 system were performed using a high pressure experimental chamber (HPEC) made with Ti-V-Al (6AL 4V ELI, ASTM Grade 5) alloy (Guggenheim and Koster van Groos, 2014). The HPEC interior is interconnected by two horizontal and two vertical channels. One of the vertical channels allows X-rays to pass through via a pair of opposing diamond windows, 1 mm apart. The other vertical channel contains an internal pump that maintains a suspension of the smectite–brine–CO_2 mixture while X-ray data were collected. The suspension is produced by the rapid flow rate caused by the narrow space between the diamond windows. The rapid flow rate also allowed rapid mixing and equilibration. The HPEC allows study of smectite in suspension while XRD data are being collected. The HPEC resolves problems on studying smectites that flocculate under brine solutions, as well as problems on low signal-to-noise ratio caused by X-ray dispersion from the liquid.

Experimental procedure

CaSWy-2 or MgSWy-2 was loaded in the HPEC with brine solutions corresponding to the interlayer cation (e.g. $CaCl_2$ brine with CaSWy-2). This procedure avoids cation exchange if brines of a different or mixed composition were used. $CaCl_2$ or $MgCl_2$ brine solutions at varying concentrations (0.17 M, 0.34 M, 0.68 M, 1.34 M, 1.71 M, 2.05 M, 3.42 M, and saturated) were made using high-purity (99.99%) salts. The brine solutions were prepared on the day of the experiment. In variable-pressure experiments, X-ray data were initially collected under ambient conditions before increasing the CO_2 partial pressures ($P(CO_2)$) to 30, 70, 100, 200, 300, 400, and 500 bars at a constant temperature (T) of approximately 33°C. In temperature experiments, X-ray data were also collected under ambient conditions before increasing the $P(CO_2)$ to 250 bars at T ~33°C. The temperature was then increased to 50, 75, 100, 125, and 150°C, and $P(CO_2)$ was allowed to vary. The experimental $P(CO_2)$ and T range were chosen to include *in situ* formation $P(CO_2)$ and T of naturally occurring CO_2 reservoirs (Miocic et al., 2016). Prior to collecting the X-ray data for each experiment, the clay suspension was circulated for 30 min so that the system could reach equilibrium.

Data collection

The HPEC loaded with 200 mg of sample and 2–3 mL of brine was mounted on a Bruker D8 3-circle transmission mode X-ray diffractometer; the diffractometer is equipped with a PHOTON 100 CMOS area detector (1024×1024 pixels) at a distance of 120 mm from the sample center, a Monocap collimator with a 0.3° divergence, and a graphite monochromator. The diffractometer was operated at 45 kV and 25 mA with a Mo X-ray tube.

The pressure in the HPEC was monitored with a transducer, and the temperature with a thermocouple, external from the brine but within the HPEC body, located 1 mm from the diamond windows (see Guggenheim and Koster van Groos, 2014). Data frames were collected for 1200 s (20 min) using Bruker APEX3 (version 2019.11-0) software. To generate the intensity *vs* 2θ diffraction plot, the frames were processed using the Bruker application GADDS (version 4.1.60, 2017). The diffraction plot was calibrated using the (003), (004), and (005) peaks of Ag(I)-behenate. The Ag(I)-behenate was loaded in the HPEC with distilled H_2O and was analyzed similar to the samples. The d_{001} value at full-width half-maximum was obtained from the diffraction plot imported to Materials Data Inc. *JADE*+ (version 9.6.0, 2015).

Geochemical modeling

Extent of dissolution

The reaction of SWy-2, brine, and CO_2 was modeled using the numerical model code *PHREEQC* v.3.7.3 (Parkhurst and Appelo, 2013) with the database from the Lawrence Livermore National Laboratory dataset (llnl.dat). The phase Montmor-*X* [$X^{y}_{0.33/y}Mg_{0.33}Al_{1.67}Si_4O_{10}(OH)_2$], where *X* is the interlayer cation Na^+, Ca^{2+} or Mg^{2+} and y is the charge of the ion in the database, was used to model SWy-2. The rate equation used to model the dissolution of SWy-2 was derived from the transition state theory (TST) rate law (Aagaard and Helgeson, 1982; Hellevang *et al.*, 2013):

$$r = Sk\prod_i a_i^{v_+}(1-\Omega), \quad (1)$$

where r is the reaction rate (mol s^{-1}), S is the reactive surface area (m^2), k is the far-from-equilibrium dissolution rate coefficient (mol m^{-2} s^{-1}), a is the activity of species i, v_+ is the reaction order, and Ω is the saturation state expressed as the exponential of the Gibbs free energy of the reaction over the gas constant and absolute temperature [exp(ΔG/RT)]. The dissolution rate coefficient parameters for SWy-2 were obtained from Palandri and Kharaka (2004) using the acid mechanism parameters for montmorillonite. Because the parameters from Palandri and Kharaka (2004) are pH dependent, the activity product term in Eqn 1 is defined by the pH of the solution. The reactive surface area was approximated by:

$$S = nM\beta, \quad (2)$$

where n is the number of moles, M is the molecular weight (g mol^{-1}) and β is the specific surface area (m^2 g^{-1}). The value of β was obtained from Golubev et al. (2006).

PHREEQC uses the ideal gas law to compute the solubility of gases in solution. To model the solubility of CO_2, the input $P(CO_2)$ values were corrected using a fugacity coefficient computed using the Soave–Redlich–Kwong (SRK) equation of state (Soave, 1972) and a Poynting correction term. The resulting solubility of CO_2 with these corrections is in good agreement with the solubility computed using the model of Duan and Sun (2003) (Hellevang and Kvamme, 2007). The equilibrium constant (K) of dissociation for all reactions performed in PHREEQC was based on the following equation:

$$\log K = a + bT + \frac{c}{T} + d\log T + \frac{e}{T^2} \quad (3)$$

where K is the equilibrium constant, and a, b, c, d, and e are constants. The constants for each phase are included in the llnl.dat database.

Prior to computing the extent of dissolution of SWy-2, pH values were calculated using the corrected CO_2 solubility at 3.00 M NaCl brine under different CO_2 pressures [$P(CO_2)$] at 40 and 75°C. The calculated pH values are in good agreement

with experimental values from Shao et al. (2013). The extent of dissolution of SWy-2 was modelled using the XRD experimental $P(CO_2)$, T and brine composition and concentration as the initial conditions. The model simulated the length of the one experiment, 1 h, after which the SWy-2 was no longer reacting.

Swelling pressure

The swelling pressures were calculated based on the extended Derjaguin–Landau–Verwey–Overbeek (DLVO) model by Liu (2013). The DLVO model approximates σ as the sum of the osmotic repulsive pressure (P_{osm}), the van der Waals attractive pressure (P_{vdW}), and the hydration pressure (P_{hyd}):

$$\sigma = P_{osm} + P_{vdW} + P_{hyd} \quad (4)$$

where P_{osm}, P_{vdW}, and P_{hyd} are calculated using Eqn (5), (6), and (7), respectively:

$$P_{osm} = \frac{RT}{V_{H_2O}} \ln[a(H_2O)], \quad (5)$$

$$P_{vdW} = -\frac{A}{6\pi h^3} \quad (6)$$

and

$$P_{hyd} = Kexp\left(-\frac{h}{\lambda}\right) \quad (7)$$

where R is the gas constant, T is the temperature in Kelvin, V_{H_2O} is the molar volume of water, A is the Hamaker constant, h is the thickness of the interlayer, and K and λ are constants. The values of A, K, and λ were obtained from Liu (2013), and h is calculated by the difference of the d_{001} values of SWy-2 and its dehydrated thickness, 9.6 Å (Ferrage et al., 2007).

Results

Effect of brine composition and concentration

The effect of varying $CaCl_2$ and $MgCl_2$ brine concentrations from 0.17 M to saturation on the interlayer distance of CaSWy-2 and MgSWy-2, respectively, were examined and compared with the effect of NaCl brines on Na-rich SWy-2 (hereafter Na-SWy-2) (Benavides et al., 2020) (Fig. 1). Both CaSWy-2 and MgSWy-2 results showed trends similar to the Na-SWy-2 results. In general, as brine concentration increases, the d_{001} value decreases along with noticeable sharp decreases. In the CaSWy-2 experiments, a sharp d_{001} decrease from 18.8 to 15.6 Å (18%) is observed when the brine concentration was increased from 0.68 to 1.71 M. In contrast, for MgSWy-2 the sharp d_{001} decrease occurred at a higher concentration. The largest d_{001} value decrease from 19.0 to 15.6 Å (18%) was observed when the brine concentration was increased from 1.37 to 3.42 M for MgSWy-2, which is similar to the decrease for Na-SWy-2. The corresponding d_{001} values of CaSWy-2 are approximately 0.4 Å lower compared with MgSWy-2 and Na-SWy-2. At lower brine concentrations (<0.34 M), d_{001} values for both CaSWy-2 and MgSWy-2 do not exceed 20.1 Å, which is the greatest d_{001} value observed for Na-SWy-2. The d_{001} values in CaSWy-2 and MgSWy-2 reach a value of 15.1 Å at saturation.

Effect of CO_2 pressure

Figure 2 shows that the effect of increasing $CaCl_2$ brine concentration with increasing $P(CO_2)$ to 500 bars at T of approximately 33°C on the d_{001} value of CaSWy-2. The gap between 0.68 and 1.71 M corresponds to the steep slope in Fig. 1. At lower brine concentrations (<0.38 M), the d_{001} values remain the same within the standard error when $P(CO_2)$ is increased from ambient pressure to 500 bars. In general, when the $P(CO_2)$ is increased from ambient pressures to 500 bars, there is no change in the d_{001} values observed for CaSWy-2 in $CaCl_2$ brines.

The d_{001} values of MgSWy-2 change with increasing $P(CO_2)$, as shown in Fig. 3. The gap between 1.37 and 3.42 M corresponds to the steep slope in Fig. 1, similar to the CaSWy-2 experiments.

For brine concentrations <1.37 M, the d_{001} values of MgSWy-2 decrease from 19.2 to 18.9 Å (2%) when $P(CO_2)$ is increased to 500 bars. Between 1.37 and 3.42 M, an increase in the d_{001} value is observed when $P(CO_2)$ is increased to approximately 30 bars, then the d_{001} values remain the same when $P(CO_2)$ is increased to 500 bars. For example, at a brine concentration of 2.05 M at

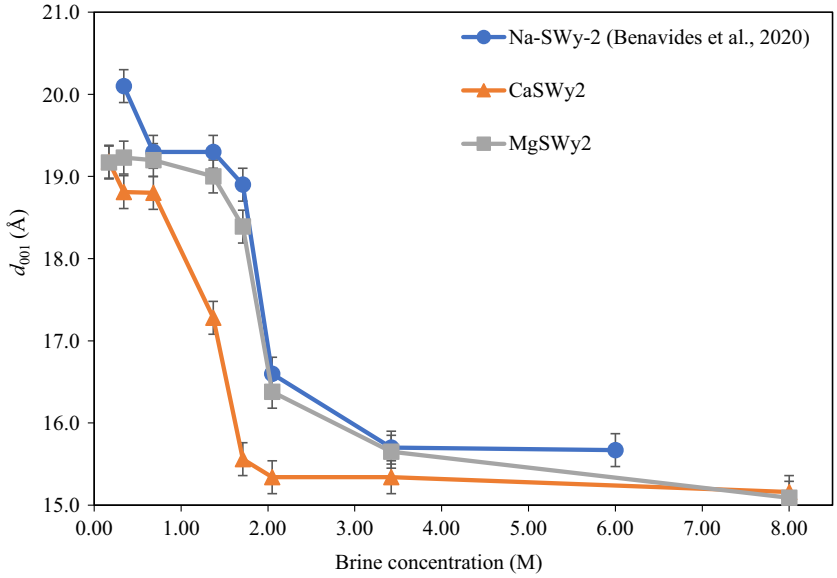

Figure 1. Effect of brine composition and concentration on the d_{001} value of SWy-2 at $P(CO_2)$ of 30 bars and T of approximately 33°C. The brine composition corresponds to the interlayer cation (e.g. $CaCl_2$ brine with CaSWy-2). The d_{001} value error bars are ±0.2 Å.

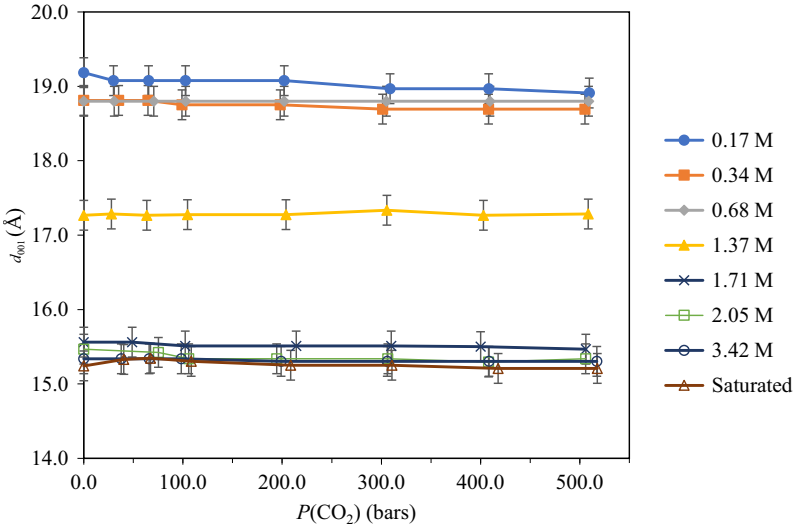

Figure 2. Effect of $CaCl_2$ brine concentration and CO_2 pressure ($P(CO_2)$) on the d_{001} of CaSWy-2 at T of approximately 33°C. The d_{001} error bars are ±0.2 Å.

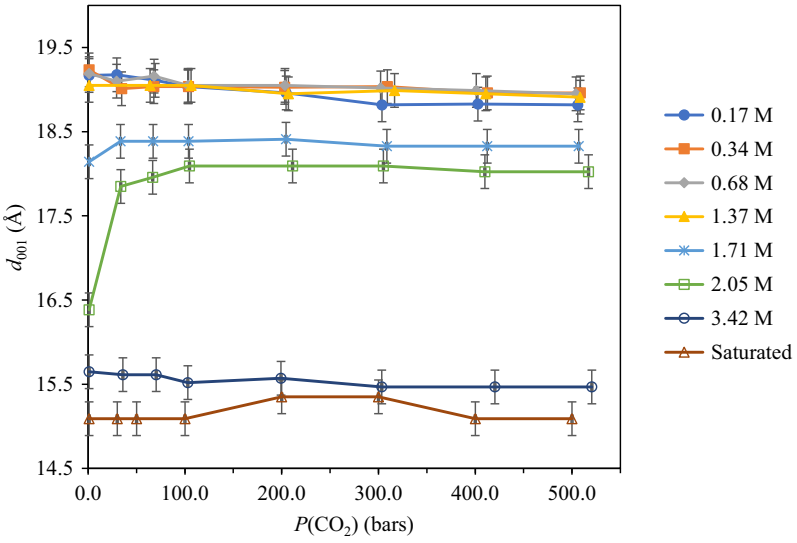

Figure 3. Effect of $MgCl_2$ brine concentration and CO_2 pressure ($P(CO_2)$) on the d_{001} of MgSWy-2 at T of approximately 33°C. The d_{001} error bars are ±0.2 Å.

ambient conditions, the d_{001} value of MgSWy-2 is 16.4 Å. When $P(CO_2)$ is increased to 30 bars, the d_{001} values increased to 17.9 Å and remained the same within the standard error when $P(CO_2)$ is increased to 500 bars. At brine concentration >3.42 M, the d_{001} values remain within the standard error when the $P(CO_2)$ is increased from ambient conditions to 500 bars.

Effect of temperature

The effect of varying $CaCl_2$ brine concentrations and increasing T to 150°C on the d_{001} value of CaSWy-2 is shown in Fig. 4. The starting $P(CO_2)$ prior to increasing T is 250 bars. At brine concentrations of <2.05 M, a decreasing trend in the d_{001} values is observed as T increases to 150°C. The greatest decrease is observed at a brine concentration of 1.37 M. As T increases from 50 to 105°C, the d_{001} value decreases from 17.1 to 15.4 Å (11%). As the brine concentration increases, the sharp decrease in d_{001} values occurs at a lower T. For example, the d_{001} value starts to decrease at 125°C at 0.68 M, in contrast to the 1.37 M concentration where the d_{001} starts to decrease at 50°C. At brine concentrations of <0.68 M, the T where the d_{001} value sharply decreases probably occurs beyond the experimental T, 150°C. At brine concentrations of >1.71 M, d_{001} values remain within the standard error when T is increased to 150°C.

The d_{001} values of MgSWy-2 at varying $MgCl_2$ brine concentrations show similar trends to those of CaSWy-2 when T is increased to 150°C (Fig. 5). However, at brine concentrations of ≤3.42 M, the sharp decrease in d_{001} values for MgSWy-2 as T is increased to 150°C is not as apparent as those of CaSWy-2. At brine concentrations of ≤2.05 M, the sharp decrease in the d_{001} values probably occurs at T beyond the experimental temperature of 150°C. For example, at brine concentration of 2.05 M, the d_{001} is beginning to decrease at T of 100°C, and might decrease sharply at a T greater than 150°C. At saturation, the d_{001} values are within the standard error when T is increased to 150°C.

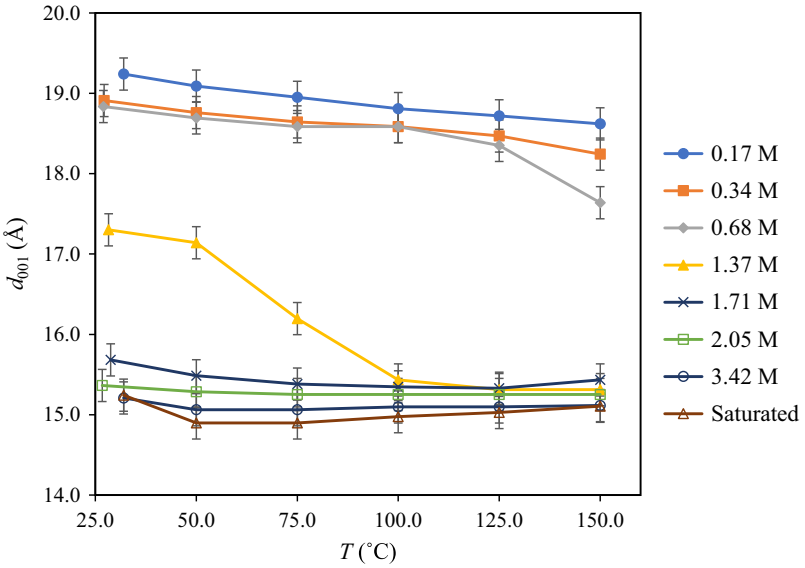

Figure 4. Effect of $CaCl_2$ brine concentration and temperature (T) on the d_{001} of CaSWy-2. The observed $P(CO_2)$ recorded for each T is shown below the T axis. The $P(CO_2)$ is a dependent variable. The d_{001} error bars are ±0.2 Å.

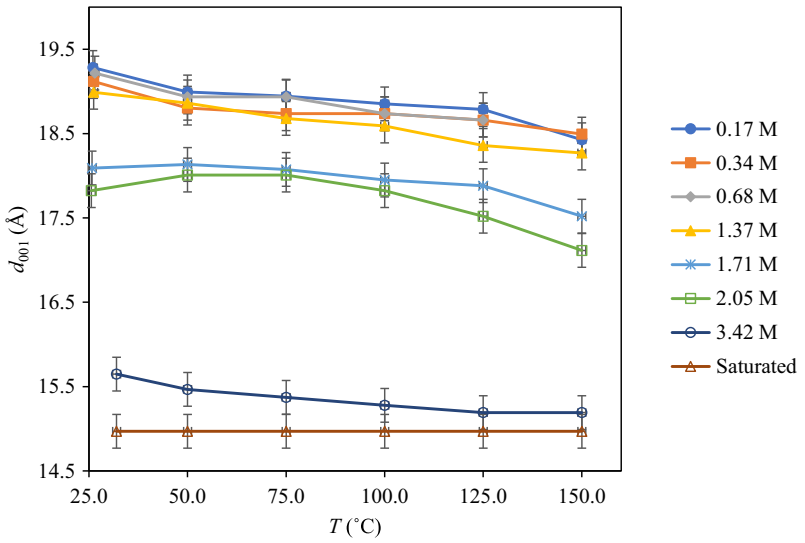

Figure 5. Effect of $MgCl_2$ brine concentration and temperature (T) on the d_{001} of MgSWy-2. The observed $P(CO_2)$ recorded for each T is shown below the T axis. The $P(CO_2)$ is a dependent variable. The d_{001} error bars are ±0.2 Å.

Swelling pressures

Figure 6 shows the effect of the swelling pressures (σ) on the d_{001} of Na-SWy-2 in NaCl brines with data from Benavides et al. (2020), and CaSWy-2 and MgSWy-2 in $CaCl_2$ and $MgCl_2$ brines, respectively, from this study. Regression coefficients for the linear relationships are summarized in Table 1. The hydration states with three planes of H_2O [3W, d_{001}=18.5–19.5 Å] and two planes of H_2O [2W, d_{001}=13.9–15.8 Å] and their corresponding d_{001} value ranges are highlighted in gray. The d_{001} value range for the 2W hydration state in Fig. 6 is only from 14.5 to 15.8 Å. The d_{001} value range for the 2W hydration state is based on best-fit modeling on SWy-2 obtained by Ferrage et al. (2005), whereas the range for the 3W is based on this study.

In all experiments, the d_{001} values decrease as σ increases. The transition from a 3W to a 2W hydration state occurs at different swelling pressures for the three sets of experiments. The σ where the 3W–2W transition begins was estimated from the d_{001} value range midpoint for the hydration state, e.g. d_{001}=19.0 Å for 3W. The transition for Na-SWy-2 experiments occurs at approximately σ=7.04 MPa, whereas the transition for CaSWy-2 and MgSWy-2 experiments occurs at approximately σ=7.68 and σ=7.74 MPa, respectively. Only Na-SWy-2 has d_{001} values greater than that for a 3W hydration state, and the 3W to a higher hydration state begins at approximately σ=7.04 MPa.

Extent of dissolution of SWy-2 in experiments

The calculated pH and percentage of dissolved SWy-2 for each $P(CO_2)$ (Fig. 7) and temperature (Fig. 8) are presented. The data include different brine compositions and concentration experiments from Benavides et al. (2020) for Na-SWy-2 in NaCl

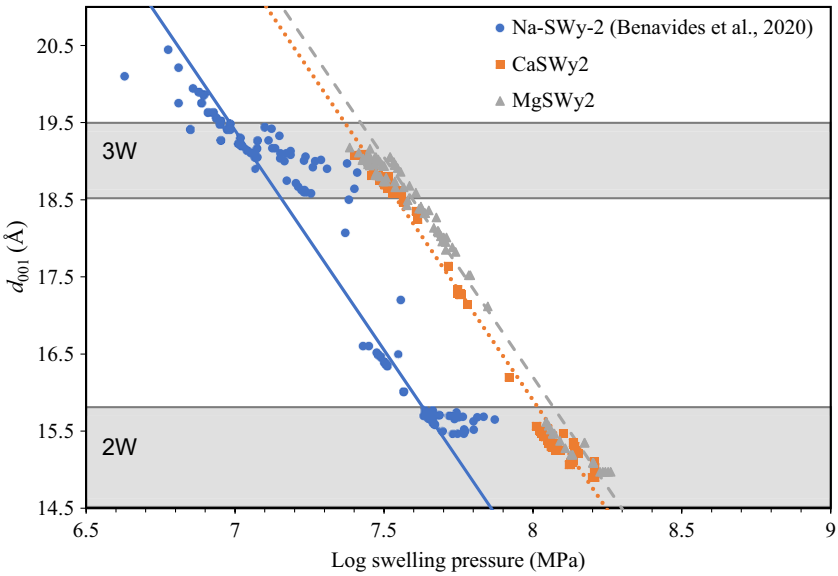

Figure 6. Effect of the calculated log swelling pressure on the d_{001} values of SWy-2. The circles represent Na-SWy-2 in NaCl brine experiments with data from Benavides et al. (2020). The squares and triangles represent CaSWy-2 and MgSWy-2 in $CaCl_2$ and $MgCl_2$ brine experiments in this study, respectively. The continuous, dotted, and dashed lines represent the best linear fit for Na-SWy-2, CaSWy-2, and MgSWy-2 experiments, respectively. The d_{001} value ranges for the 3W and 2W hydration states are highlighted in gray, and the d_{001} value range for 2W does not show values from 13.9 to 14.5 Å. Errors are not given because of the data point density.

Table 1. Linear regression coefficients for the Na-SWy-2, CaSWy-2, and MgSWy-2 plots in Fig. 6

	Slope	Intercept	R^2
Na-SWy-2	–5.7	59.3	0.98
CaSWy-2	–5.7	61.5	0.99
MgSWy-2	–5.7	61.8	0.91

brines, and from this study for CaSWy-2 in $CaCl_2$ brines and MgSWy-2 in $MgCl_2$ brines. The percentage of dissolved SWy-2 is the percentage difference of the initial mass of Na-SWy-2, CaSWy-2, or MgSWy-2, and their mass at steady state.

Pressure

In all brine compositions and at all concentrations, as $P(CO_2)$ increases, pH rapidly decreases from 30 to 70 bars and slowly decreases from 70 to 500 bars. Also, pH decreases as the brine concentration increases from 0.17 to 3.42 M (Fig. 7A,C,E). An opposite trend is observed for the percentage of dissolved SWy-2. The percentage of dissolved SWy-2 rapidly increases as $P(CO_2)$ increases from 30 to 70 bars, and the percentage of dissolved SWy-2 slowly increases from 70 to 500 bars. As brine concentration increases from 0.17 to 3.42 M, the percentage of dissolved SWy-2 also increases (Fig. 7B,D,F).

The MgSWy-2 in $MgCl_2$ brine experiments exhibit the lowest pH range values, of 3.07–3.51 (Fig. 7E). However, the pH ranges for CaSWy-2 in $CaCl_2$ brines (Figure 7C) and Na-SWy-2 in NaCl brines (Fig. 7A) are similar with range values of 3.20–3.60 and 3.25–3.67, respectively. A different trend is observed for the percentage of dissolved SWy-2. The highest percentage of dissolved SWy-2 range is observed with CaSWy-2 in $CaCl_2$ brine experiments from 0.38 to 1.04% (Fig. 7D), followed by MgSWy-2 in $MgCl_2$ brine experiments from 0.30 to 0.82% (Fig. 7F). The lowest percentage of dissolved SWy-2 range is observed with Na-SWy-2 in NaCl brine experiments with values ranging from 0.30 to 0.61% (Fig. 7B).

Temperature

As the temperature is increased from 50 to 150°C, pH decreases for all sets of experiments (Fig. 8A,C,E). However, for Na-SWy-2 in NaCl brine experiments, the pH decreases when the temperature is increased from 100 to 150°C, with the exception of 3.42 M. At these concentrations, the pH values start increasing again when temperature is increased from 100 to 150°C (Fig. 8A). In contrast to $P(CO_2)$, the percentage of dissolved SWy-2 shows a similar trend with pH. As temperature is increased from 50 to 150°C, the percentage of dissolved SWy-2 decreases for all sets of experiments (Fig. 8B,D,F). In all experiments, pH decreases when the brine concentration increases, whereas the percentage of dissolved SWy-2 increases.

Discussion

Effects of P(CO_2), temperature, and brine concentration

Benavides et al. (2020) examined the effect of NaCl brines on the d_{001} of Na-SWy-2 and found that as brine concentration increases, the d_{001} value decreases, with the greatest decrease observed at concentrations between 1.37 and 2.05 M. Furthermore, those authors observed that the transition from osmotic swelling to intracrystalline swelling of Na-SWy-2 occurred when the brine concentration was increased from 0.17 to 0.34 M. Osmotic swelling results from the chemical potential difference between the brine and the interlayer, whereas intracrystalline swelling is a stepwise change in hydration state in the interlayer. The present study also shows that for CaSWy-2 and MgSWy-2, the d_{001}value decreases as the brine concentration increases. However, in CaSWy-2 and MgSWy-2 experiments, only intracrystalline swelling is observed, where the hydration state in the interlayer changed from 3W to 2W with increasing brine concentration. The concentration of cations in the clay silicate layer is fixed to satisfy the layer charge, whereas the concentration in solution depends on the brine concentration. When the brine concentration is increased, the ions in solution compete for the H_2O molecules around the

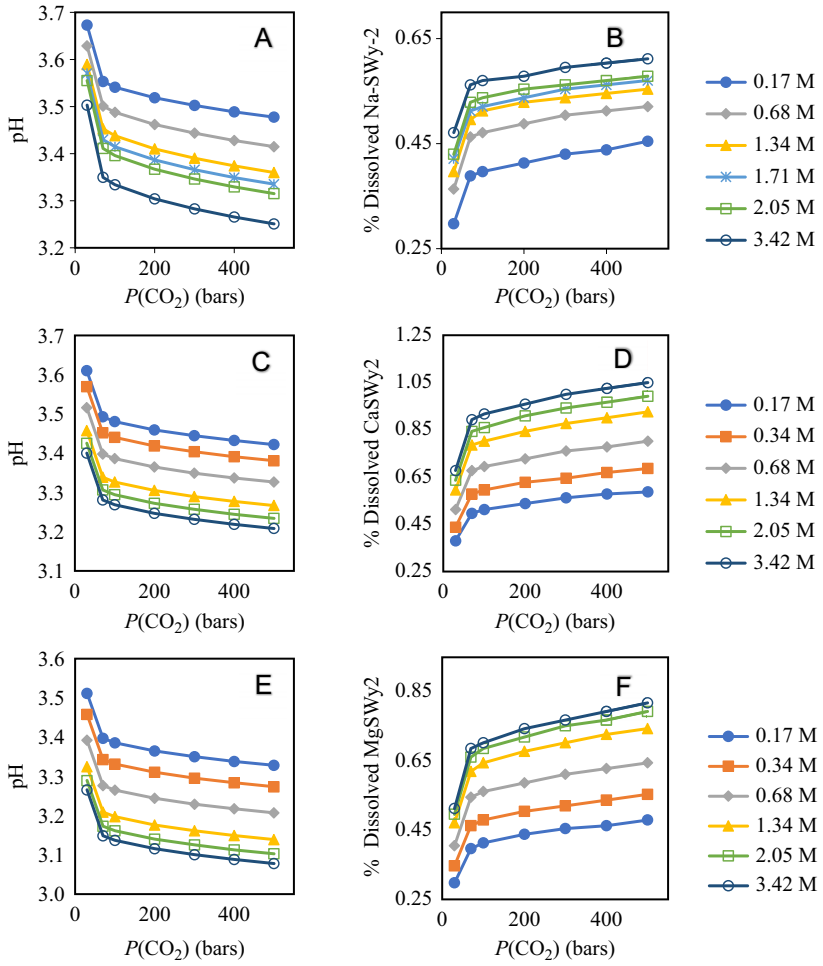

Figure 7. Calculated pH and percentage of dissolved SWy-2 under different CO_2 pressure ($P(CO_2)$) and brine composition and concentration experimental conditions for Na-SWy-2 in NaCl brines (A,B) with data from Benavides et al. (2020), and CaSWy-2 in $CaCl_2$ brines (C,D) and MgSWy-2 in $MgCl_2$ brines (E,F) in this study. The percentage of dissolved SWy-2 values are the percentage difference of the initial and final amount of SWy-2 at steady state.

interlayer cation. Thus, the d_{001} value is lowered from that corresponding to a 3W hydration state as the H_2O molecules leave the interlayer. Furthermore, the d_{001} values at a 3W hydration state are greater in comparison with the d_{001} values found in Ferrage et al. (2005) (e.g. 18.0–18.5 Å). These higher d_{001} values in the present study are attributed to the experimental set-up, where the SWy-2 particles were allowed to flow freely in the suspension, thereby allowing the SWy-2, brine, and CO_2 to achieved equilibrium rapidly. Intermediate d_{001} values between 2W and 3W hydration states are also observed for both CaSWy-2 and MgSWy-2 experiments. Intermediate d_{001} values result from increased ion–ion interactions in the interlayer as brine concentration increases. This would be expected to affect the position of the H_2O molecules around the cation in the interlayer.

The d_{001} values sharply decreased from 18.8 to 15.6 Å at 1.25 M for CaSWy-2 in $CaCl_2$ brines, and from 19.0 to 15.6 Å at 1.50 M for MgSWy-2 in $MgCl_2$ brines (Fig. 1). Slade and Quirk (1991) investigated the effect of varying $CaCl_2$ and $MgCl_2$ solutions on the intracrystalline swelling of different smectites, including SWy-2. The results in the present study are consistent with the results obtained by Slade and Quirk (1991). The sharp decrease in the d_{001} value occurs at 1.37 M for MgSWy-2 in $MgCl_2$ brine experiments, which is in good agreement with Slade and Quirk (1991) at 1.50 M. However, in CaSWy-2 in $CaCl_2$ brine experiments, the sharp decrease in the d_{001} value occurs at 0.68 M, which is lower than Slade and Quirk (1991) at 1.25 M. This difference is attributed to the gentler slope in the initial d_{001} decrease between 0.68 and 1.37 M. The sharp d_{001} decrease may occur closer to 1.37 M if the CaSWy-2 experiments follow the sharp decrease trend observed in the Na-SWy-2 and MgSWy-2 experiments.

Effect of interlayer cation

The interlayer cation affects the d_{001} value (Fig. 1) and swelling pressure (Fig. 6) of SWy-2. In experiments with divalent cations (Ca^{2+} and Mg^{2+}), only intracrystalline swelling is observed with the stepwise change in hydration level at the transition brine concentration, whereas with Na, osmotic swelling is observed at concentrations less than 0.34 M (Benavides et al., 2020). This swelling is consistent with literature data for experiments in which clays were oriented on slides (e.g. Ferrage et al., 2005), or prepared as thin films (e.g. Slade et al., 1991). Furthermore, in MgSWy-2 experiments done at brine concentrations of 1.71 and 2.05 M, the d_{001} value increases when $P(CO_2)$ is increased from ambient conditions to 30 bars at T approximately 33°C (Fig. 3). The d_{001} value at ambient conditions is probably metastable. The initial

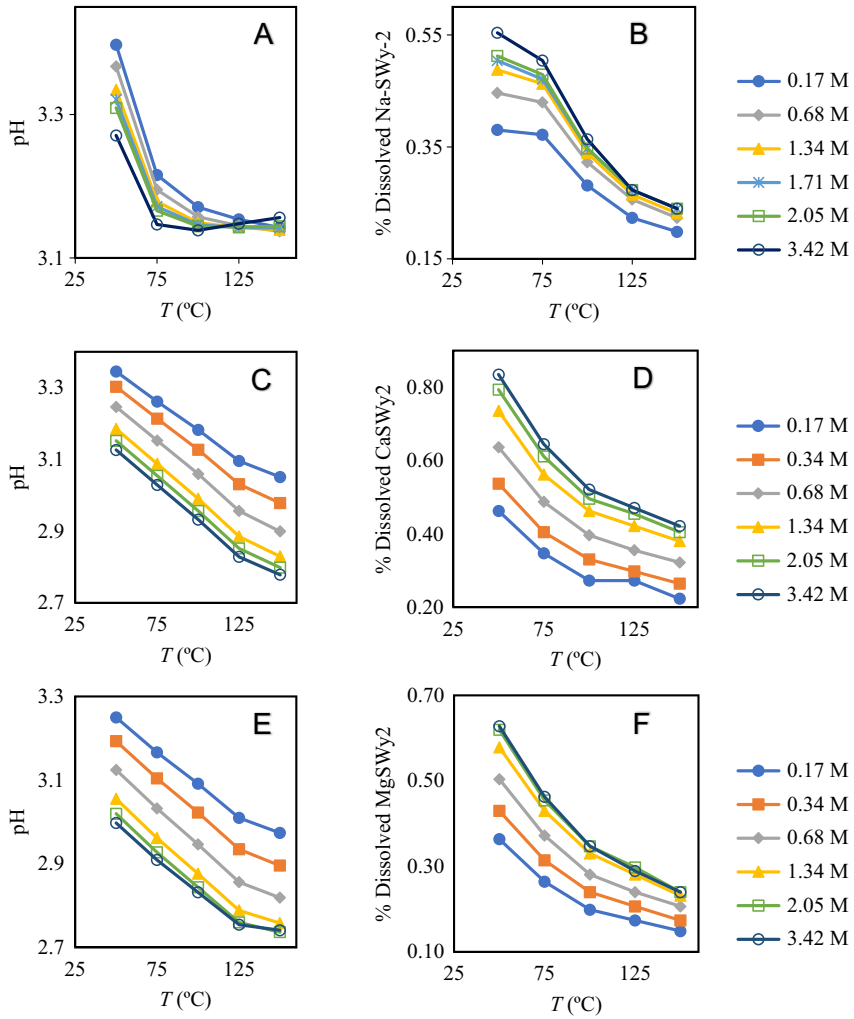

Figure 8. Calculated pH and percentage of dissolved SWy-2 under different temperature (*T*) and brine composition and concentration experimental conditions for Na-SWy-2 in NaCl brines (A,B) with data from Benavides et al. (2020), and CaSWy-2 in $CaCl_2$ brines (C,D) and MgSWy-2 in $MgCl_2$ brines (E,F) in this study. The percentage of dissolved SWy-2 values are the percentage difference of the initial and final amount of SWy-2 at steady state.

low d_{001} value is probably a result of the temperature increase caused by the exothermic reaction when the $MgCl_2$ brine was prepared, which effectively shift this experimental point to a higher temperature (Fig. 4).

The difference in the d_{001} values for the different cations under similar $P(CO_2)$, *T*, and brine concentration (e.g. 19.3, 19.2, and 18.8 Å for Na-SWy-2, CaSWy-2, and MgSWy-2, respectively, at $P(CO_2)$ = 30 bars, *T* = approximately 33°C, and brine concentration = 0.68 M) at a 3W hydration level is a result of the hydration energy of the cations, and how the cations are coordinated with the silicate layer (outer-sphere or inner-sphere complex). The higher d_{001} values for Na-SWy-2 probably occur because of the tendency of Na cations near the silicate layer to form outer-sphere complexes, where the coordinated H_2O molecules around the cation are retained, whereas the cations for CaSWy-2 and MgSWy-2 form inner-sphere complexes, where the cations are directly coordinated with the silicate layer (Planková and Lísal, 2020). Furthermore, the charge density of Ca and Mg is greater than that of Na, and so the show a greater attraction for the negatively charged silicate layers. Hence, CaSWy-2 and MgSWy-2, in general, have smaller d_{001} values compared with Na-SWy-2 for the same brine concentration.

At 3W and 2W hydration levels, the d_{001} values are approximately 0.4 Å higher for MgSWy-2 than for CaSWy-2 (Figs 1, 2, and 3) because of the difference in the hydration energy of the interlayer cations. The hydration energy, which depends on the charge and size of the cation, influences the ability of a cation to attract H_2O molecules. The more negative hydration energy of Mg (–1920 kJ mol^{-1}) is smaller compared with Ca (–1560 kJ mol^{-1}) and Na (–410 kJ mol^{-1}) (Smith, 1977). Hence, MgSWy-2 is likely to attract more H_2O molecules into the interlayer, causing greater expansion, i.e. higher d_{001} values, compared with CaSWy-2. The hydration energy is also consistent with the range of swelling pressures over which the 3W to 2W hydration level transition occurs (Fig. 6). Among the three experiments, MgSWy-2 transitions with the highest swelling pressure at 7.74 MPa followed by CaSWy-2 at 7.68 MPa, then Na-SWy-2 at 7.04 MPa.

Calculated pH

The calculated pH for all experiments decreases when $P(CO_2)$ is increased to 500 bars (Fig. 7A,C,E) or *T* is increased to 150°C (Fig. 8A,C,E). The decrease in pH results from dissolved CO_2

reacting with H_2O to form H_2CO_3 that can dissociate to produce H^+ ions. The concentration of dissolved CO_2 increases as $P(CO_2)$ increases, and a decrease is observed when temperature and brine concentration are increased (Duan and Sun, 2003). The decrease in the calculated pH when $P(CO_2)$ is increased is a result of an increase in dissolved CO_2 in the solution. The rapid decrease in pH occurs when $P(CO_2)$ is increased to 70 bars because CO_2 is in the gas phase. However, the slow decrease in pH (up to 0.10 pH units) when $P(CO_2)$ is increased from 70 to 500 bars occurs because the CO_2 is the supercritical phase. This trend is observed at all brine compositions and concentrations and is consistent with the trend observed by Shao et al. (2013) with their pH values obtained experimentally.

The increase in temperature in closed-system experiments is also accompanied by an increase in $P(CO_2)$, which allows more CO_2 to dissolve in the brine to result in a decrease in pH. However, the trend of the pH decrease changes when temperature is increased from 100 to 150°C in NaCl brine experiments (Fig. 8A). This occurs because less H^+ is produced, i.e. the pH is higher, although the brine composition and concentration also affects the pH values. Hence, changes in $P(CO_2)$, temperature, and brine composition and concentration affect the calculated pH of the solution.

Dissolution of SWy-2

When $P(CO_2)$ is increased to 500 bars (Fig. 7B,D,F), the observed increase in percentage of dissolved SWy-2 is a result of the decreased pH of the brine. A decrease in pH corresponds to an increase in H^+ activity $a(H^+)$. The complete dissolution reaction of SWy-2 can be expressed as:

$$X^{y}_{0.33/y}Mg_{0.33}Al_{1.67}Si_4O_{10}(OH)_2 + 6.00H^+ \rightarrow 0.33/yX^y + 0.33Mg^{+2} + 1.67Al^{+3} + 4.00H_2O + 4.00SiO_2, \quad (8)$$

where X is the interlayer cation (Na^+, Ca^{+2}, Mg^{+2}) and y is the charge of the ion. The increase in the $a(H^+)$ will cause the reaction to proceed to the right. However, the percentage of dissolved SWy-2 decreases for all experiments despite the decrease in pH when T is increased to 150°C (Fig. 8). This result is related to the decrease in solubility of SWy-2 when temperature is increased, i.e. retrograde solubility. The equilibrium constant for the complete dissolution of SWy-2 (Eqn 8) decreases when temperature is increased and results in the reaction favoring the reactants, i.e. decrease in solubility of SWy-2.

The percentage of dissolved SWy-2 from the models for all experiments ranges from 0.2 to 1.1% for a pH range of 2.74–3.67 (Figs 7 and 8). The low percentage of dissolved SWy-2 in acidic conditions is consistent with kinetic experiments of K-exchanged montmorillonite dissolution in KCl solutions at T=23±1°C obtained by Zysset and Schindler (1996). The total amount of K-exchanged montmorillonite dissolved in their experiments ranged from 0.46% (pH 4.0) to 6.09% (pH 1.0). Zysset and Schindler (1996) attributed this low value to dissolution that occurred mostly at edge sites (Si-O-Al or Al-OH-Al) and not at basal sites. The mechanism of dissolution occurs by protonation of the edge sites. Under acidic conditions, the density of protonated edge sites (>$AlOH^{2+}$) increases (Stadler and Schindler, 1993). The increase in protonated edge sites leads to the detachment of an Al^{3+}-proton complex followed by hydrolysis of the tetrahedral sheet. Furthermore, the detached transition-state complex acts as a limiting step for the dissolution reaction (Huertas et al., 1999).

Conclusions and implications

The present study shows that changes in environmental conditions affect the interlayer distance, i.e. the d_{001} value, of CaSWy-2-$CaCl_2$ and MgSWy-2-$MgCl_2$ brine systems, which is consistent with results from the study of Na-SWy-2 in NaCl brines by Benavides et al. (2020). Overall, the d_{001} value of SWy-2 changes significantly when brine concentration and T are varied, whereas little to no change was observed when $P(CO_2)$ is varied. When brine concentration is increased from 0.17 M to saturation, the d_{001} value of CaSWy-2-$CaCl_2$ and MgSWy-2-$MgCl_2$ brines systems can decrease by 18% at 0.68 and 1.37 M, respectively. Furthermore, both brine systems show that the d_{001} value can decrease by up to 11% when T is increased from approximately 33 to 150°C; however, the d_{001} value decrease in MgSWy-2-$MgCl_2$ brine systems is less apparent. The difference in results in both brine systems occurs because of the difference in hydration energies of the interlayer cation, where Mg has a greater hydration energy than Ca. Thus, a greater brine concentration and T are needed to decrease the d_{001} values of MgSWy-2. This observation is consistent with the swelling pressures (σ) needed to change the hydration state of SWy-2 from 3W to 2W.

Geochemical modeling was used to simulate how SWy-2 will react under XRD experimental conditions until SWy-2 no longer reacts. When $scCO_2$ is injected into the HPEC, the pH of the brine decreases as a result of the dissolution of CO_2 in the solution. The decrease in pH produces more H^+, which causes SWy-2 to dissolve. The decrease in pH is associated with an increase in percentage of dissolved SWy-2 because there are more H^+ ions reacting with SWy-2. However, the inverse is observed with a pH decrease when T increases to 150°C. The inverse is attributed to the retrograde solubility of SWy-2, i.e. SWy-2 is less soluble at higher T. In general, the modeling shows that the pH decrease only results in a low dissolution of SWy-2 of up to 1.1% dissolved SWy-2.

The range of *P-T* conditions in the present study included *in situ P-T* conditions of naturally occurring saline aquifers (Miocic et al., 2016). Overall, under the short-term stratigraphic and structural trapping mechanism, the interlayer distance, d_{001} value, changes in smectite, such as SWy-2, can result in changes in the porosity and/or permeability of a saline aquifer and a caprock. When the d_{001} value of smectite increases, the saline aquifer becomes less porous and less permeable and results in a decrease in its capacity to store CO_2. In contrast, this will enhance the sealing capacity of a caprock. However, a decrease in the d_{001} value of smectite might result in an increase in porosity and permeability. Thus, the saline aquifer benefits because an increase in the CO_2 storage capacity of the aquifer occurs, whereas for a caprock, the same result may create conduits for CO_2 to escape to the surface. However, when CO_2 injection stops, geochemical trapping becomes the dominant mechanism of sequestering CO_2. The stored CO_2 in the aquifers will decrease the brine pH, which results in the dissolution of smectite until it reaches a steady state. Smectite will probably continue to be present in the reservoir rock because of its low solubility.

Smectite has a wide range of silicate-layer compositions affecting its layer charge location and density, which also affect its d_{001} value with changes in $P(CO_2)$, T, and brine concentration, and its extent of dissolution. Experimental work coupled with modeling of smectite with different silicate-layer compositions and appropriate brines and other minerals present are essential for full assessment of the stability of smectites in saline aquifer-caprock systems. In addition, the parameter of 'time' (i.e. reaction kinetics) needs to be

considered in the modeling because CO_2 containment (e.g. geochemical trapping) may require long-term storage, perhaps hundreds or thousands of years.

Author contributions. Paolo Andre Benavides: Conceptualization, Formal Analysis, Funding Acquisition, Investigation, Methodology, Visualization, and Writing; Stephen Guggenheim: Conceptualization, Methodology, Project Administration, Supervision, Resources, and Writing.

Acknowledgements. The authors thank August Koster Van Groos and Kathryn Nagy for reviewing the manuscript, and Richard Dojutrek for laboratory assistance.

Financial support. The Authors acknowledge the funding provided by the University of Illinois at Chicago Chancellor's Graduate Research Award, The Clay Minerals Society Student Research Grant, and the Department of Earth and Environmental Sciences, University of Illinois at Chicago.

Competing interests. The authors declare that they have no known competing financial interests or personal relationships that could have appeared to influence the work reported in this paper.

Data availability statement. The data used to support the findings of this study are available from the corresponding author, PAB, upon request.

References

Aagaard, P., & Helgeson, H.C. (1982). Thermodynamic and kinetic constraints on reaction rates among minerals and aqueous solutions; I. *Theoretical considerations*. American Journal of Science, *282*, 237–285. doi: 10.2475/ajs.282.3.237

Baker, J.C., Uwins, P.J.R., & Mackinnon, I.D. (1993). ESEM study of illite/smectite freshwater sensitivity in sandstone reservoirs. *Journal of Petroleum Science and Engineering*, *9*, 83–94. doi: 10.1016/0920-4105(93)90069-Q

Benavides, P.A., Kowalik, J., Guggenheim, S., & Koster van Groos, A.F. (2020). Effect of CO_2 pressure, temperature, and brine composition on the interlayer spacing of Na-rich and K-exchanged montmorillonite. *Applied Clay Science*, *198*, 105819. doi: 10.1016/j.clay.2020.105819

Davidson, J., Freund, P., & Smith, A. (2001). Putting carbon back in the ground. *The IEA Greenhouse Gas R&D Programme.*

Duan, Z., & Sun, R. (2003). An improved model calculating CO_2 solubility in pure water and aqueous NaCl solutions from 273 to 533 K and from 0 to 2000 bar. *Chemical Geology*, *193*, 257–271. doi: 10.1016/S0009-2541(02)00263-2

Ferrage, E., Lanson, B., Sakharov, B.A., & Drits, V.A. (2005). Investigation of smectite hydration properties by modeling experimental X-ray diffraction patterns: Part I. Montmorillonite hydration properties. *American Mineralogist*, *90*, 1358–1374. doi: 10.2138/am.2005.1776

Ferrage, E., Lanson, B., Sakharov, B.A., Geoffroy, N., Jacquot, E., & Drits, V.A. (2007). Investigation of dioctahedral smectite hydration properties by modeling of X-ray diffraction profiles: influence of layer charge and charge location. *American Mineralogist*, *92*, 1731–1743. doi: 10.2138/am.2007.2273

Friedlingstein, P., O'Sullivan, M., Jones, M.W., Andrew, R.M., Hauck, J., Olsen, A., Peters, G.P., Peters, W., Pongratz, J., Sitch, S., Le Quéré, C., Canadell, J.G., Ciais, P., Jackson, R.B., Alin, S., Aragão, L.E.O.C., Arneth, A., Arora, V., Bates, N.R., Becker, M., Benoit-Cattin, A., Bittig, H.C., Bopp, L., Bultan, S., Chandra, N., Chevallier, F., Chini, L.P., Evans, W., Florentie, L., Forster, P.M., Gasser, T., Gehlen, M., Gilfillan, D., Gkritzalis, T., Gregor, L., Gruber, N., Harris, I., Hartung, K., Haverd, V., Houghton, R.A., Ilyina, T., Jain, A.K., Joetzjer, E., Kadono, K., Kato, E., Kitidis, V., Korsbakken, J.I., Landschützer, P., Lefèvre, N., Lenton, A., Lienert, S., Liu, Z., Lombardozzi, D., Marland, G., Metzl, N., Munro, D.R., Nabel, J.E.M.S., Nakaoka, S.-I., Niwa, Y., O'Brien, K., Ono, T., Palmer, P.I., Pierrot, D., Poulter, B., Resplandy, L., Robertson, E., Rödenbeck, C., Schwinger, J., Séférian, R., Skjelvan, I., Smith, A.J.P., Sutton, A.J., Tanhua, T., Tans, P.P., Tian, H., Tilbrook, B., van der Werf, G., Vuichard, N., Walker, A.P., Wanninkhof, R., Watson, A.J., Willis, D., Wiltshire, A.J., Yuan, W., Yue, X., & Zaehle, S. (2019). Global carbon budget 2019. *Earth System Science Data*, *11*, 1783–1838. doi: 10.5194/essd-12-3269-2020

Giesting, P., Guggenheim, S., Koster van Groos, A.F., & Busch, A. (2012a). X-ray diffraction study of K-and Ca-exchanged montmorillonites in CO_2 atmospheres. *Environmental Science & Technology*, *46*, 5623–5630. doi: 10.1021/es3005865

Giesting, P., Guggenheim, S., Koster van Groos, A.F., & Busch, A. (2012b). Interaction of carbon dioxide with Na-exchanged montmorillonite at pressures to 640 bars: implications for CO_2 sequestration. *International Journal of Greenhouse Gas Control*, *8*, 73–81. doi: 10.1016/j.ijggc.2012.01.011

Golubev, S.V., Bauer, A., & Pokrovsky, O.S. (2006). Effect of pH and organic ligands on the kinetics of smectite dissolution at 25C. *Geochimica et Cosmochimica Acta*, *70*, 4436–4451. doi: 10.1016/j.gca.2006.06.1557

Gregersen, U., Johannessen, P.N., Møller, J.J., Kristensen, L., Christensen, N.P., Holloway, S., Chadwick, A., Kirby, G., Lindberg, E., & Zweigel, P. (1998). *Saline Aquifer CO_2 Storage SACS Phase Zero* 1998.

Guggenheim, S., & Koster van Groos, A. F. (2014). An integrated experimental system for solid-gas-liquid environmental cells. *Clays and Clay Minerals*, *62*(6), 470–476.

Hellevang, H., & Kvamme, B. (2007). ACCRETE – an explicit algorithm to solve kinetically constrained CO2-water-rock interactions. In *Proceedings of the 3rd WSEAS International Conference on Mathematical Biology and Ecology, Gold Coast, Queensland, Australia, January* (pp. 17–19).

Hellevang, H., Pham, V.T., & Aagaard, P. (2013). Kinetic modelling of CO_2–water–rock interactions. *International Journal of Greenhouse Gas Control*, *15*, 3–15. doi: 10.1016/j.ijggc.2013.01.027

Huertas, F.J., Chou, L., & Wollast, R. (1999). Mechanism of kaolinite dissolution at room temperature and pressure. Part II: Kinetic study. *Geochimica et Cosmochimica Acta*, *63*, 3261–3275. doi: 10.1016/S0016-7037(99)00249-5

Ilgen, A.G., & Cygan, R.T. (2016). Mineral dissolution and precipitation during CO_2 injection at the Frio-I Brine Pilot: geochemical modeling and uncertainty analysis. *International Journal of Greenhouse Gas Control*, *44*, 166–174. doi: 10.1016/j.ijggc.2015.11.022

IPCC (2007). Climate change 2007: synthesis report. In Core Writing Team, Pachauri, R.K., Reisinger, A. (eds), Contribution of Working Groups I, II and III to the Fourth Assessment Report of the Intergovernmental Panel on Climate Change. Intergovernmental Panel on Climate Change, Geneva, Switzerland, 104 pp.

Liu, L. (2013). Prediction of swelling pressures of different types of bentonite in dilute solutions. *Colloids and Surfaces A: Physicochemical and Engineering Aspects*, *434*, 303–318. doi: 10.1016/j.colsurfa.2013.05.068

Loring, J.S., Schaef, H.T., Thompson, C.J., Turcu, R.V., Miller, Q.R., Chen, J., Hu, J., Hoyt, D., Martin, P., Ilton, E., Felmy, A., & Rosso, K.M. (2013). Clay hydration/dehydration in dry to water-saturated supercritical CO_2: implications for caprock integrity. *Energy Procedia*, *37*, 5443–5448. doi: 10.1016/j.egypro.2013.06.463

Miocic, J.M., Gilfillan, S.M., Roberts, J.J., Edlmann, K., McDermott, C.I., & Haszeldine, R.S. (2016). Controls on CO_2 storage security in natural reservoirs and implications for CO_2 storage site selection. *International Journal of Greenhouse Gas Control*, *51*, 118–125. doi: 10.1016/j.ijggc.2016.05.019

Michael, K., Golab, A., Shulakova, V., Ennis-King, J., Allinson, G., Sharma, S., & Aiken, T. (2010). Geological storage of CO_2 in saline aquifers – a review of the experience from existing storage operations. *International Journal of Greenhouse Gas Control*, *4*, 659–667. doi: 10.1016/j.ijggc.2009.12.011

Moore, D.M., & Reynolds Jr, R.C. (1997). *X-ray Diffraction and the Identification and Analysis of Clay Minerals*. Oxford University Press. doi: 10.1346/CCMN.1990.0380416

Norrish, K. (1954). The swelling of montmorillonite. *Discussions of the Faraday Society*, *18*, 120–134. doi: 10.1039/DF9541800120

Palandri, J.L., & Kharaka, Y.K. (2004). *A compilation of rate parameters of water-mineral interaction kinetics for application to geochemical modeling*. Geological Survey Menlo Park, CA.

Parkhurst, D.L., & Appelo, C.A.J. (2013). User's guide to PHREEQC (version 2): a computer program for speciation, batch-reaction, one-dimensional transport, and inverse geochemical calculations. *Water-Resources Investigations Report*, *99*, 312. doi: 10.3133/wri994259

Planková, B., & Lísal, M. (2020). Molecular dynamics of aqueous salt solutions in clay nanopores under the thermodynamic conditions of hydraulic fracturing:

Interplay between solution structure and molecular diffusion. *Fluid Phase Equilibria*, *505*, 112355. doi: 10.1016/j.fluid.2019.112355

Sato, T., Watanabe, T., & Otsuka, R. (1992). Effects of layer charge, charge location, and energy change on expansion properties of dioctahedral smectites. *Clays and Clay Minerals*, *40*(1), 103–113.

Shao, H., Thompson, C.J., Qafoku, O., & Cantrell, K.J. (2013). *In situ* spectrophotometric determination of pH under geologic CO_2 sequestration conditions: method development and application. *Environmental Science & Technology*, *47*, 63–70. doi: 10.1021/es3016793

Slade, P. G., & Quirk, J. P. (1991). The limited crystalline swelling of smectites in CaCl2, MgCl2, and LaCl3 solutions. *Journal of Colloid and Interface Science*, *144*(1), 18–26.

Slade, P.G., Quirk, J.P., & Norrish, K. (1991). Crystalline swelling of smectite samples in concentrated NaCl solutions in relation to layer charge. *Clays and Clay Minerals*, *39*, 234–238. doi: 10.1346/CCMN.1991.0390302

Smith, D.W. (1977). Ionic hydration enthalpies. *Journal of Chemical Education*, *54*, 540. doi: 10.1021/ed054p540

Soave, G. (1972). Equilibrium constants from a modified Redlich-Kwong equation of state. *Chemical Engineering Science*, *27*, 1197–1203. doi: 10.1016/0009-2509(72)80096-4

Song, J., & Zhang, D. (2013). Comprehensive review of caprock-sealing mechanisms for geologic carbon sequestration. *Environmental Science & Technology*, *47*, 9–22. doi: 10.1021/es301610p

Stadler, M., & Schindler, P.W. (1993). Modeling of H^+ and Cu^{2+} adsorption on calcium-montmorillonite. *Clays and Clay Minerals*, *41*, 288–296. doi: 10.1346/CCMN.1993.0410303

Wigand, M., Carey, J.W., Schütt, H., Spangenberg, E., & Erzinger, J. (2008). Geochemical effects of CO_2 sequestration in sandstones under simulated in situ conditions of deep saline aquifers. *Applied Geochemistry*, *23*, 2735–2745. doi: 10.1016/j.apgeochem.2008.06.006

Zysset, M., & Schindler, P.W. (1996). The proton promoted dissolution kinetics of K-montmorillonite. *Geochimica et Cosmochimica Acta*, *60*, 921–931 doi: 10.1016/0016-7037(95)00451-3